THE JOURNAL OF PHYSICAL CHEMISTRY B

Article

pubs.acs.org/JPCB

Mesoscale Simulation of the Effect of a Lactide Segment on the Nanostructure of Star Poly(ethylene glycol-*co*-lactide)-Acrylate Macromonomers in Aqueous Solution

Seyedsina Moeinzadeh and Esmaiel Jabbari*

Biomimetic Materials and Tissue Engineering Laboratories, Department of Chemical Engineering, University of South Carolina, Columbia, South Carolina 29208, United States

ABSTRACT: The distribution of reactive groups and micelle formation in amphiphilic macromonomers and the extent of network formation in aqueous solution depend on the segment length of the hydrophobic monomer. The objective of this work was to simulate by dissipative particle dynamics (DPD) the structure of the four-arm star poly(ethylene glycol-*co*-lactide)-acrylate (SPELA) macromonomer in aqueous solution. The effect of lactide segment length (n) in each arm and macromonomer concentration on the distribution and size of the micelles was investigated. In the absence of lactide, the reactive acrylate groups were uniformly distributed in the aqueous solution. With the addition of lactide segments, micelles formed with a hydrophobic core containing lactide and acrylate beads and a hydrophilic corona of ethylene oxide beads. The size and average number of macromonomers (aggregation number) of the micelles increased with n while the number density of micelles decreased. Furthermore, the fraction of macromonomer arms incorporated in the micelles as either loops or intermicellar bridges increased with increasing n. The macromonomer bridge fraction showed a biphasic behavior with a maximum at $n = 4$. The accumulation of water beads around acrylates decreased with increasing n. The aggregation of acrylates initially increased with n, and then, it decreased for $n > 4$ due to the decrease in size and distance between the micelles. The fraction of acrylates in the core surface layer of the micelles decreased from 66 to 19% when n increased from 4 to 16 with a higher fraction of acrylates trapped in the micelles' core. Macromonomer concentration increased the number density of micelles, but it did not have a significant effect on the micelle size or distribution of the acrylates. The simulation results indicate that SPELA macromers with <4 lactide segment length can potentially produce degradable PEG-based hydrogels with the highest network density.

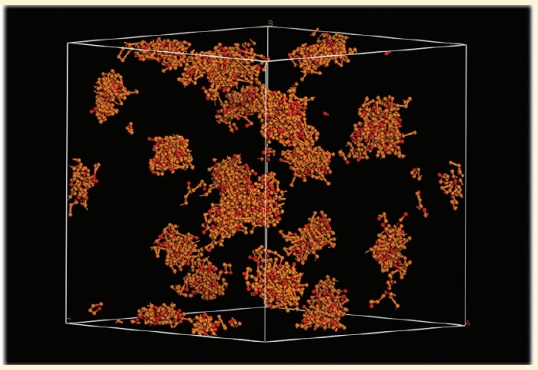

1. INTRODUCTION

Hydrogels, due to their high water content and high diffusivity of nutrients and biomolecules, are very attractive as a carrier for delivery of stem cells to the site of defect in regenerative medicine.[1−5] After injection and *in situ* hardening, the hydrogel matrix guides the development of seeded cell into the desired tissue.[6] In most *in situ* applications, the hydrogel should have robust mechanical stability to prevent deformation and rupture by soft tissue compression or other mechanical loads.[7] In addition, the hydrogel should be degradable to provide volume for tissue regeneration.[8] Hydrogels based on small-molecule monomers, due to their potentially high network density, have excellent structural stability, but viability of the seeded cells is severely reduced by the diffusion of toxic monomers across the cell membrane.[9] Naturally based injectable gels have excellent biocompatibility and support cell-matrix interaction, but they have very low cross-link density and mechanical strength.[10,11] Physically cross-linked hydrogels, due to the transient nature of the cross-links, also suffer from low mechanical strength.[12,13]

There is a need to develop synthetic biodegradable macromonomers for applications in regenerative medicine with robust mechanical properties. In that regard, hydrogels based on functionalized poly(ethylene glycol) (PEG) macromers are inert and nonimmunogenic and have a compressive modulus exceeding 1 MPa.[14,15] PEG hydrogels have been used extensively to investigate the effect of matrix physiochemical, mechanical, and biological factors on cell function *in vitro*.[7,16] To impart degradability to the hydrogels, short degradable lactide segments can be attached to the PEG macromer by ring-opening polymerization prior to acrylate functionalization to produce a degradable PEG based hydrogel.[17−19] However, the hydrophobic lactide segments in the hydrophilic PEG, in addition to reducing the solubility of the macromonomer in aqueous solution and the water content of the resulting PEG hydrogel, cause micelle formation.[20,21] Experimental results with four-arm star poly(ethylene glycol-*co*-lactide)-acrylate (SPELA) macromonomer demonstrate that the hydrogel modulus increases slightly with the addition of 1−2 lactides

Received: November 16, 2011
Revised: January 11, 2012
Published: January 11, 2012

dx.doi.org/10.1021/jp211056p | *J. Phys. Chem. B* 2012, 116, 1536−1543

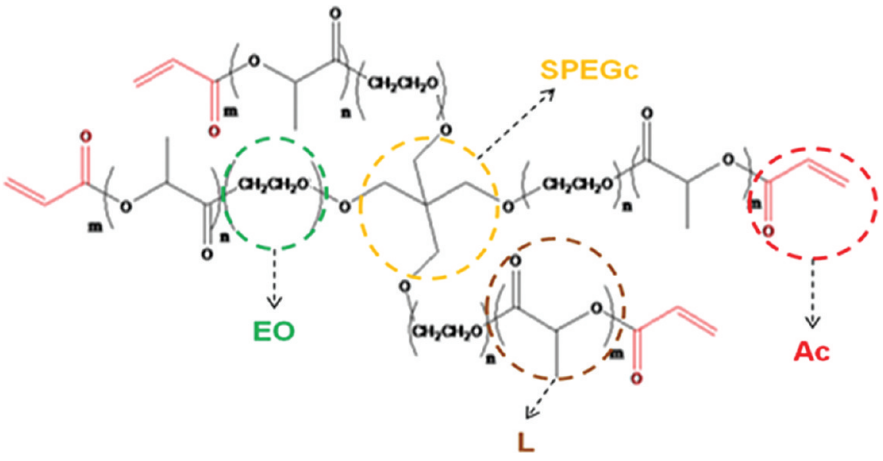

Figure 1. Bead representation of SPELA macromonomer in DPD.

per arm followed by a sharp decrease in modulus for higher lactide segment lengths.[22]

The formation of nanostructure by macromonomers in the hydrogel precursor solution alters the spatial distribution and accessibility of the reactive functional groups, which in turn affects the rate and extent of cross-linking.[23] Therefore, a molecular-scale understanding of the factors that affect nanostructure formation in these mixtures will aid us in designing hydrogels from macromonomers with improved physical and mechanical properties. Atomistic molecular simulations are limited to the atomic time and length scales.[24] Mesoscale methods in which the dynamics of the system is based on course-grained beads made up of a group of atoms have been developed to simulate the nanostructure of copolymers.[25−27] Hoogerbugge and Koelman[28] introduced the dissipative particle dynamics (DPD) approach, later revised by Espanol and Warren,[29] to simulate the dynamics of soft spherical beads interacting through pairwise additive force fields. The DPD approach has been used to simulate the mesoscale dynamics of polymer systems[30−34] after Groot and Warren related the conservative force terms to the Flory−Huggins interaction parameter.[35,36] DPD has been used to simulate the microstructure and microphase separation for linear and multiarm block copolymer mixtures and solutions.[26,37−42] The objective of this work was to simulate the nanostructure and micelle formation of SPELA macromonomer, a four-arm PEG with short lactide chains terminated with acrylates. In this work, the effect of the four-arm SPELA lactide segment length and macromonomer concentration in aqueous solution on micelle formation and distribution of the acrylate groups will be simulated with DPD. The distribution of the acrylates, namely free from the micelles, tethered, and trapped in the micelles, provide information on the cross-linking efficiency of the SPELA macromonomer and then ultimate modulus of the hydrogel.

2. METHODS

2.1. Theory. In DPD simulation, the polymer solution is divided into different beads (set of atoms) with equal mass and volume. The SPELA macromonomer is synthesized by ring-opening polymerization of lactide monomers initiated by a four-arm star PEG (MW of 5 kDa), followed by acrylation of the chain ends with acryloyl chloride. Figure 1 shows the molecular structure and different bead types on SPELA macromonomer. The bead types included lactide (L, dark brown), ethylene oxide (EO, green), acrylate (Ac, red), and star PEG center (SPEGc, light brown). Three water molecules were used for the solvent bead. The evolution of the position and velocity of all beads is governed by Newton's equation of motion:[28,29]

$$\frac{d\mathbf{r}_i}{dt} = \mathbf{v}_i, \qquad m_i\frac{d\mathbf{v}_i}{dt} = \mathbf{f}_i \tag{1}$$

where $\mathbf{r}_i$, m_i, $\mathbf{v}_i$, and $\mathbf{f}_i$ are the position vector, mass, velocity vector, and total force vector acting on bead i, respectively. The total force in a cutoff radius r_c is[29]

$$\mathbf{f}_i = \sum_{i\neq j} \mathbf{F}_{ij}^{C} + \mathbf{F}_{ij}^{D} + \mathbf{F}_{ij}^{R} \tag{2}$$

where $\mathbf{f}_i$ is the total force and $\mathbf{F}_{ij}^{C}$, $\mathbf{F}_{ij}^{D}$, and $\mathbf{F}_{ij}^{R}$ are the conservative, dissipative, and random components of the force, respectively. Different components of the force are given by[29]

$$\mathbf{F}_{ij}^{C} = \begin{cases} \alpha_{ij}(1 - r_{ij})\mathbf{e}_{ij} & r_{ij} < 1 \\ 0 & r_{ij} \geq 1 \end{cases} \tag{3}$$

$$\mathbf{F}_{ij}^{D} = -\gamma[w^{D}(r_{ij})](\mathbf{e}_{ij}\cdot\mathbf{v}_{ij})\mathbf{e}_{ij} \tag{4}$$

$$\mathbf{F}_{ij}^{R} = \sigma[w^{R}(r_{ij})]\theta_{ij}\mathbf{e}_{ij} \tag{5}$$

where r_{ij} and $\mathbf{e}_{ij}$ are the magnitude and unit vector joining bead i to j ($\mathbf{r}_{ij} = \mathbf{r}_i - \mathbf{r}_j$),$\mathbf{v}_{ij}$ is given by $\mathbf{v}_{ij} = \mathbf{v}_i - \mathbf{v}_j$, and α_{ij} is a constant that describes the maximum repulsion between the interacting beads i and j. α_{ij} which is dependent on the characteristics of the mixture (see section 2.2) plays a significant role in determining the nanostructure of the equilibrated macromonomer solution. The system contains dissipation as well as total momentum conservation due to the simultaneous action of $\mathbf{F}_{ij}^{D}$ and $\mathbf{F}_{ij}^{R}$. w^{D} and w^{R} are r-dependent weight functions for dissipative and random forces, respectively, and γ and σ are the magnitude of dissipative and random forces. θ_{ij} is a random variable with a Gaussian probability distribution. Espanol and Warren showed that the parameters for dissipative and random forces have to satisfy the fluctuation−dissipation conditions $w^{D}(r_{ij}) = [w^{R}(r_{ij})]^2$ and $\sigma^2 = 2k_BT\gamma$.[29] The optimized weight function $w^{D}(r_{ij}) = (1 - r_{ij})^2$ within the cutoff distance for soft chains in aqueous solution was used in the simulation.[36]

dx.doi.org/10.1021/jp211056p | J. Phys. Chem. B 2012, 116, 1536−1543

According to the force balance (eq 2), the beads on the macromonomer that are not directly connected move like soft spheres in the solution. However, the motion of the adjacent beads that are directly connected is constrained by covalent bonds. Thus, an additional spring force has to be included to simulate the motion of adjacent beads on the macromonomer chains. The spring force acting on the bonded consecutive beads of a chain is given by[36]

$$\mathbf{F}_i^S = \sum_j C\mathbf{r}_{ij} \tag{6}$$

where beads j are those that are connected to bead i. A value of 4 was used in the simulation for spring constant C to properly account for the distance between connected beads.[26] Due to the domination of repulsive forces between soft spheres in the mean segment length,[26] the end point distribution of the macromonomer is not very sensitive to the value of constant C.

2.2. Simulation Parameters. The parameters of the conservative force were set by choosing the mapping of three water molecules per DPD bead in order to simulate the diffusivity and compressibility of water.[43−45] This mapping made it possible to simulate the structure of SPELA macromer with small L:EO ratio and one acrylate per arm. All beads in the simulation system had the same volume of 90 Å^3 and the same mass 54 amu. By choosing the system density $\rho = 3r_c^{-3}$, the DPD fundamental length scale, r_c, was 6.46 Å and the bead−bead interaction parameters were determined by[36]

$$\alpha_{ij} = \alpha_{ii} + 3.27\chi_{ij} \tag{7}$$

where χ_{ij} is the Flory−Huggins parameter between beads i and j and α_{ii} is the repulsion parameter between beads of the same type. To satisfy the compressibility of water, the mapping of three water molecules per bead led to $\alpha_{ii} = 78$.[43] Flory−Huggins parameters were calculated using

$$\chi_{ij} = \frac{(\delta_i - \delta_j)^2 V}{RT} \tag{8}$$

where δ_i and δ_j are the solubility parameters of beads i and j, respectively, V is the bead molar volume, T is the absolute temperature, and R is the gas constant. The solubility parameters were calculated via atomistic molecular dynamics simulation (Forcite module, Materials Studio v5.5, Accelrys) using the COMPASS force field, which is an ab initio force field optimized for condensed-phase systems.[46] To arrive at the initial packing for each bead type, 64 beads were simulated in a cubic unit cell with 3D periodic boundary conditions using the rotational isomeric state (RIS) method,[47] subject to equilibration at 298 K. After geometric optimization, the unit cell was equilibrated by the annealing dynamics simulation method, which included five cycles of NVT ensemble dynamics between 300 and 800 K to prevent the system from being trapped in a local minimum. After reaching the lowest energy configuration, 1500 ps of thermalizing NPT dynamics (1 fs time step) was performed to reach the actual system temperature and pressure. Next, the cohesive energy density (CED) was determined by sampling the system and collecting data for 500 ps. The CED was related to the solubility parameter of bead i, δ_i, by

$$\delta_i = \left(\frac{\Delta H_{v,i}}{V_{m,i}}\right)^{1/2} = (\mathrm{CED})^{1/2} \tag{9}$$

where $\Delta H_{v,i}$ and $V_{m,i}$ are the molar enthalpy of vaporization and molar volume of bead i, respectively. The bead−bead repulsion parameters, α_{ij}, calculated from the solubility parameters using eqs 7 and 8, are given in Table 1.

Table 1. DPD Interaction Parameters (α_{ij}) Used in the Simulation

	Ac	L	EO	SPEGc	W
Ac	78.0	83.2	91.9	118.7	98.9
L	83.2	78.0	86.8	86.3	92.3
EO	91.9	86.8	78.0	93.3	80.5
SPEGc	118.7	86.3	93.3	78.0	115.6
W	98.9	92.3	80.5	115.6	78.0

The initial condition of each simulation was the random distribution of coarse-grained SPELA-nL macromonomers and water beads inside the simulation box with 3D periodic boundary conditions. The parameter "n" in SPELA-nL is equal to the number of L beads on each arm of the macromonomer. The total numbers of L and EO beads were held constant at 32 while n was varied, and the macromer concentration was 30% v/v unless otherwise specified. The macromonomer was simulated in cubic boxes with lengths of $30r_c$, $40r_c$, and $50r_c$. The relative distribution and structure of the macromonomer after equilibration was independent of size of the simulation box. The simulated root-mean-square radius of gyration (R_g) of the four-arm PEG (MW of 5.9 kDa with 33 beads on each arm) was 25.4 Å, which was in the theoretical range 21.2−27.8 Å.[48,49] Furthermore, the length of the simulation box (197 Å for $30r_c$) was an order of magnitude larger than R_g, indicating that the finite size effects may have no effect on our results.[42] Bead diffusivities reached steady-state values after 150000 time steps. All simulations ran 200000 times with a dimensionless time step of 0.05. For each sample, the DPD simulation was repeated five times (with randomly seeded macromonomers in the simulation box) and the results were reported as the mean ± standard deviation. All atomistic and mesoscale calculations were performed via the Amorphous Cell, Forcite, and Mesocite modules of Materials Studio v5.5 (Accelrys, San Diego, CA).[50]

3. RESULTS AND DISCUSSION

3.1. Effect of Lactide Fraction. Figure 2 shows the effect of the number of lactides on structure formation of SPELA-nL macromers in water (30% v/v). It should be noted that the W, EO, and SPEGc beads are not shown in Figure 2 for clarity. In the absence of lactide ($n = 0$), the acrylates were uniformly distributed over the volume of the simulation box. Addition of lactide segments ($n \geq 2$) to the macromonomer led to the formation of micellar structures. The hydrophobic lactide and acrylate beads of the arms belonging to different macromonomers aggregated and formed the core of the micelles while the hydrophilic EO segments, facing the aqueous phase, formed the micelle's corona. Those arms that are not part of the hydrophobic core of the micelles are referred to as "free arms". With increasing number of lactides per arm, the core size of the micelles increased while the number of free arms decreased.

A cross section of the structures, corresponding to those in Figure 2, is shown in Figure 3. With increasing n, more arms of each macromonomer participated in the formation of the micellar core. Consequently, the core size increased with n while the corona thickness decreased, as shown in Figure 3. At

dx.doi.org/10.1021/jp211056p | J. Phys. Chem. B 2012, 116, 1536−1543

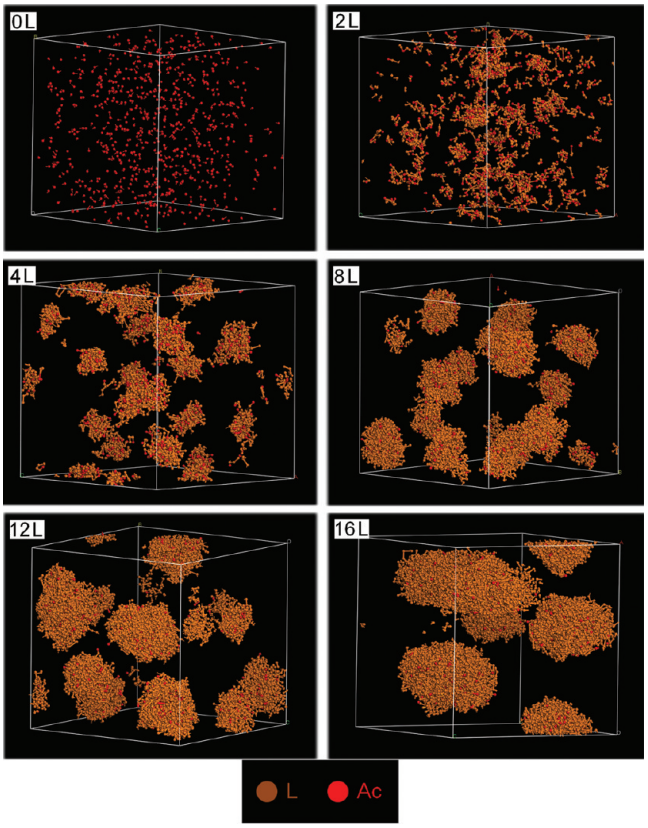

Figure 2. Evolution of micellar cores for SPELA-*n*L macromonomers in 30% aqueous solution. "L" and "Ac" represent lactide and acrylate beads, respectively. The other beads in the image are not shown for clarity.

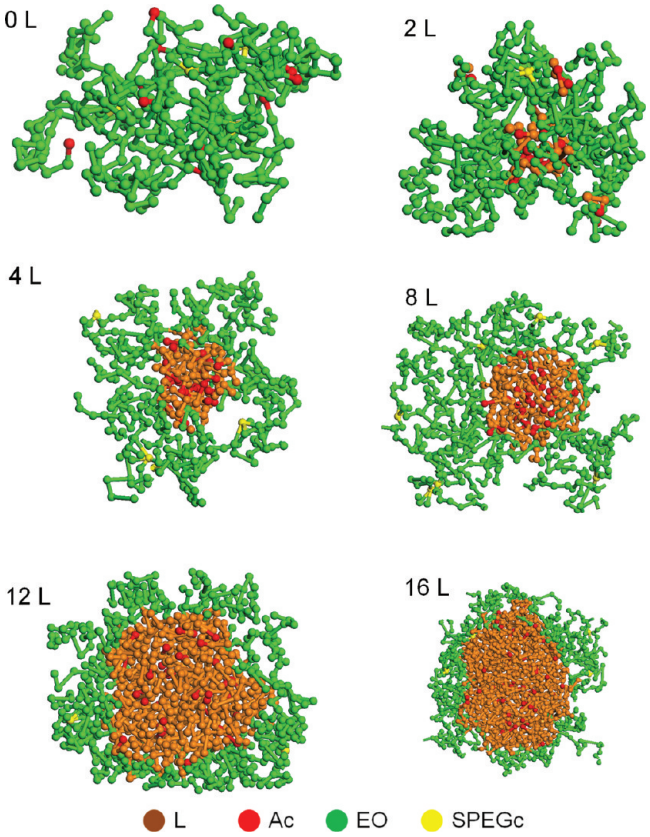

Figure 3. Cross section of the micelles for SPELA-*n*L macromonomers in 30% aqueous solution. "L", "Ac", "EO", and "SPEGc" represent lactide, acrylate, ethylene oxide, and the star PEG core, respectively. The water beads are not shown for clarity.

low n with small hydrophobic domains, the EO segments had an extended conformation in the aqueous phase at the water–micelle interface. However, as n and the volume of the hydrophobic domain increased, the EO segments adopted a 2D stretched conformation on the surface of the micelles. This change in conformation is caused by repulsive interactions between water and lactide segments at the interface dominating over the reduction in entropy as the EO segments adopt a 2D conformation on the micelle surface.

The effect of number of lactides on each arm on the core radius and number density of micelles is shown in Figure 4a. The core size increased with the volume fraction of lactide segments, while the number density decreased. Although the aggregation of lactide segments and formation of micelles reduces the total free energy of the solution, two positive contributions to the free energy controlled the core size and number density.[51] One factor is the free energy of the water–micelle interface, which is proportional to the core surface area per macromonomer. The other factor is the steric repulsive energy between the hydrophilic EO segments positioned at the corona–core interface of the micelles, which is inversely proportional to the core surface area per macromer. The number of EO beads per unit core surface area deceases with increasing n, leading to a decrease in repulsive energy between the EO segments. At the same time, the EO layer thickness on the core surface decreases with increasing n, thus leading to an increase in interfacial free energy. Since the core size increased with n (see Figures 2 and 3), the net effect is the domination of interfacial over repulsive free energy, which led to the formation of micelles with smaller core surface areas per molecule, larger cores, and lower number density of micelles.

The average number of SPELA macromonomers in a micelle or aggregation number, n_{agg}, can be calculated by the following equation, assuming there are only L and Ac beads in the micelle's core:

$$n_{agg} = \frac{\rho V_c}{4(n+1)} \tag{10}$$

where ρ and V_c are the bead number density and micelle core volume, respectively. Figure 4b shows that the aggregation number increased with n. According to Figure 4b, there was a sharp increase in n_{agg} from 3 to 9 when n was raised from 2 to 4. That increase can be related to the transition from macromonomer density fluctuation (size < R_g) to micelle formation (see Figure 2). n_{agg} also increased sharply when n was raised from 12 to 16, which can be related to the transition from micellar to microphase separated solution. For the case of SPELA-20L, the small interfacial surface area per macromonomer could not be achieved for minimization of free energy by spherical packing, which led to the formation of continuous phases in the simulation box (data not shown).

3.2. Effect of Macromonomer Concentration. The effect of macromonomer concentration on core radius and number density of micelles for SPELA-4L is shown in Figure 5. The core radius slightly increased from 14.9 to 16 Å as the SPELA concentration was increased from 5 to 30%. The ratio of water to lactide beads was higher for lower SPELA concentrations, resulting in a stronger repulsive interaction at

dx.doi.org/10.1021/jp211056p | J. Phys. Chem. B 2012, 116, 1536–1543

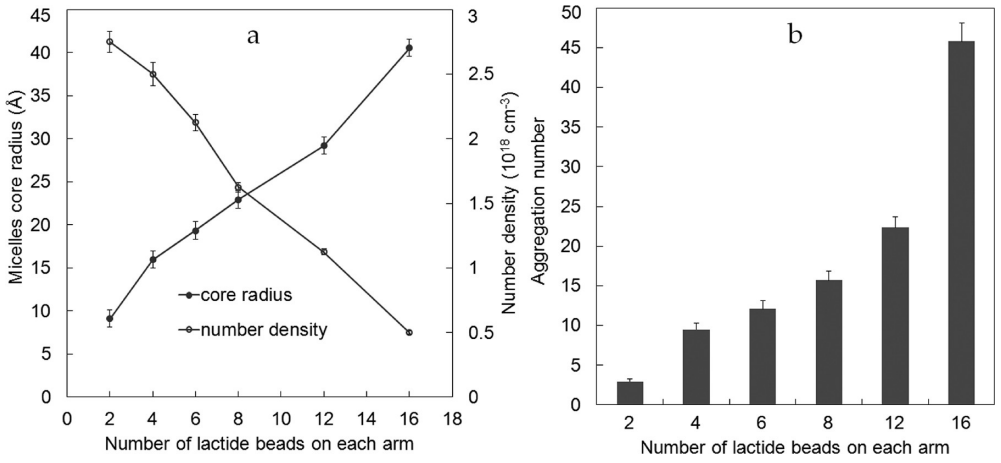

Figure 4. The effect of the number of lactide beads on each arm on (a) the micelle core size and number density and (b) the aggregation number of micelles in 30% aqueous solution of SPELA-*n*L macromonomers. *n* represents the number of lactide beads on each macromonomer arm, which has a total of 32 L and EO beads. Error bars correspond to means ± 1 SD for $n = 5$ simulations.

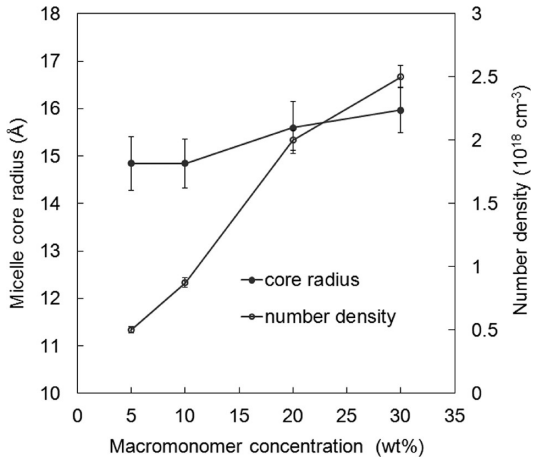

Figure 5. The effect of macromonomer concentration on the core size and number density of the micelles in aqueous solution of SPELA-4L macromonomers. Error bars correspond to means ± 1 SD for $n = 5$ simulations.

the micelle–water interface and smaller core size. Since there was a slight change in core size with concentration, the number density of micelles increased with increasing macromonomer concentration. In addition, the distribution of acrylates in the core of the micelles did not change significantly with increasing SPELA concentration.

3.3. Inter-Micellar Bridging. The cross sections in Figure 3 show that the center of the macromonomers (SPEGc) is positioned in the corona of the micelles. Therefore, the arms can possess three different conformations, namely, the intermicellar bridges, loops in which at least two arms of a macromonomer are in the same micelle, and free arms. The three conformations are shown schematically in Figure 6. For SPELA-0L with $n = 0$, the arms are in solution and considered free. For SPELA macromonomer with $n > 0$, aggregation of hydrophobic lactide groups and micelle formation results in the creation of loops and bridges. Assuming ideal solution and connectivity of the macromonomer arms does not affect partitioning, the relation between the mole fraction of arms in the micelles (X_{ma}) and free arms (X_{fa}) at thermodynamic equilibrium is given by[52]

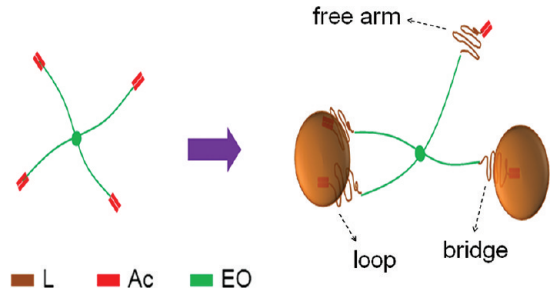

Figure 6. Schematic representation of bridge, loop ,and free arm conformations of SPELA macromonomers in aqueous solution. "L", "Ac", and "EO" represent lactide, acrylate, and ethylene oxide beads, respectively.

$$\frac{ln(X_{ma})}{4n_{agg}} = -\frac{\mu^0_{mic} - \mu^0_f}{RT} + ln(X_{fa}) + \frac{ln(4n_{agg})}{4n_{agg}} \qquad (11)$$

where $(\mu^0_{mic} - \mu^0_f)$ are the standard chemical potential of micellization per arm, n_{agg} is the aggregation number of macromonomers in a micelle, and R and T are the gas constant and absolute temperature, respectively. According to Figure 5, macromonomer concentration has a slight effect on micelle core size and thus the aggregation number. Therefore, on the basis of eq 11, the fraction of free arms, X_{fa}, does not change significantly with an increase in the total macromonomer concentration $X_T = X_{ma} + X_{fa}$. However, it significantly increases the fraction of arms with bridge and loop conformation. Therefore, there is a smaller fraction of free arms and larger fraction of loops and bridges at higher macromonomer concentrations. As the ratio of L to EO increases at constant X_T, the fraction of free arms decreases.

The number of bridges per micelle and the bridge fraction of the arms as a function of *n* are shown in Figure 7. The number of bridges per micelle continuously increased with *n*, while the bridge fraction showed a biphasic behavior. The bridge fraction initially increased when *n* increased from 2 to 4, which can be attributed to the decrease in the fraction of free arms from 70 to 14% of total arms. With increasing *n* to values >4, the intermicellar distance increased while the length of hydrophilic EO segments connecting the micelles decreased, thus reducing the probability of bridge formation and the bridge fraction.

dx.doi.org/10.1021/jp211056p | J. Phys. Chem. B 2012, 116, 1536–1543

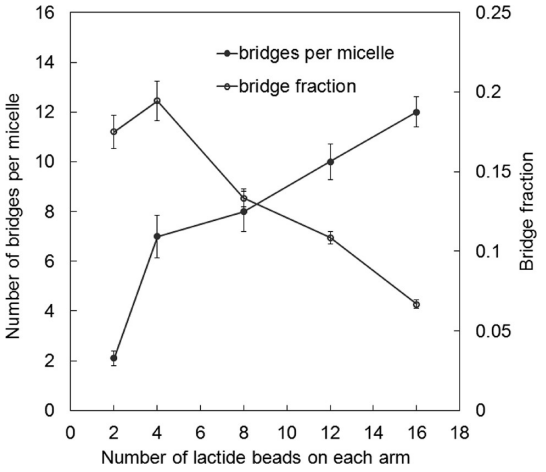

Figure 7. The effect of the number of lactide beads on each arm on the number of bridges per micelle and bridge fraction in 30% aqueous solution of SPELA-*n*L macromonomers. Error bars correspond to means ± 1 SD for n = 5 simulations.

The contribution of each bridge to the elastic modulus of the physically formed network is related to the residence time of the arm in the micelle's core, which is proportional to[53]

$$\tau \sim \gamma \cdot n^{2/3} \tag{12}$$

where γ is the effective interfacial tension between the micelle's core and solution. With increasing n, the EO segments adopt a thinner interfacial layer on the core surface with lower entropy, thus increasing the interfacial tension of the micelle−water interface. Therefore, both n and γ increased the residence time of the bridges with increasing number of lactides per arm. As a result, the contribution of each bridge to the elastic modulus of the network increased with n[54] even though the fraction and number density of bridges decreased for $n > 4$. That effect, in turn, reduced the mobility and accessibility of the reactive acrylate groups with increasing n.

3.4. Distribution of Reactive Acrylate Beads. The reactivity of an acrylate group in the macromonomer depends on its mobility and its proximity to other acrylates in the solution. The acrylate mobility, in turn, depends on the concentration of water in the microenvironment. To quantify the proximity of an acrylate bead to water beads or other acrylate beads, the average number of water (n_{Ac-w}) or acrylate (n_{Ac-Ac}) beads in a sphere of radius R around an acrylate bead or the running integration number of beads "a" around beads "b", $n_{ab}(R)$, was calculated by[55]

$$n_{ab}(R) = 4\pi\rho_{b0}\int_0^R g_{ab}(r)r^2\,dr \tag{13}$$

where ρ_{b0} is the overall number density of beads of type "b" and $g_{ab}(r)$ is the radial distribution function of bead "b" around bead "a", located at the origin.[56] The effect of the number of lactides in the SPELA macromonomer on n_{Ac-w} and n_{Ac-Ac} in a radius of 20 Å is shown in Figure 8a and b, respectively. n_{Ac-w} increased with radial distance, but the SPELA-0L macromonomer (n = 0) had the highest integration number with maximum coverage of acrylate groups by water beads. With increasing n and formation of larger lactide cores, the fraction of hydrophobic acrylates facing water decreased, leading to a decrease in n_{Ac-w}. The n_{Ac-w} value for SPELA-0L at radial distance r_c was an order of magnitude higher than that of SPELA-16L. This large difference emphasizes the higher accumulation of water beads around acrylates, and hence higher accessibility to the aqueous phase, for macromonomers with a low number of lactides. According to Figure 8b, SPELA-0L with the most uniform distribution of acrylate beads had the lowest n_{Ac-Ac}. The hydrophilic EO segments in SPELA-0L served as an energy barrier against the formation of acrylate aggregates; thus, the acrylate local density was the same as the overall density. Increasing n and the phase separation of lactide and acrylate beads led to an increase in n_{Ac-Ac}, as shown in Figure 8b. As n increased from 0 to 2 and 4, the fraction of macromonomer arms incorporated in the micelles increased from 0 to 30 and 86%, respectively, which led to a higher local density of acrylates and a decrease in the average Ac−Ac bead distance. With further increase in n, the local density of acrylates in the micelles' core decreased and the intermicellar distance increased which led to an overall decrease in n_{Ac-Ac} for $n > 4$. Therefore, n_{Ac-Ac} reached a maximum value for n = 4.

Figure 9 shows the effect of n on the radial distribution of acrylates in the core of micelles. Due to its hydrophobic nature, there was a high density of acrylate beads in the central part of the micelles' core. However, a significant fraction of acrylate beads in micelles with smaller cores, due to volume constraints, were positioned near the surface layers. For example, in SPELA-4L with relatively smaller core size, 66% of the acrylates

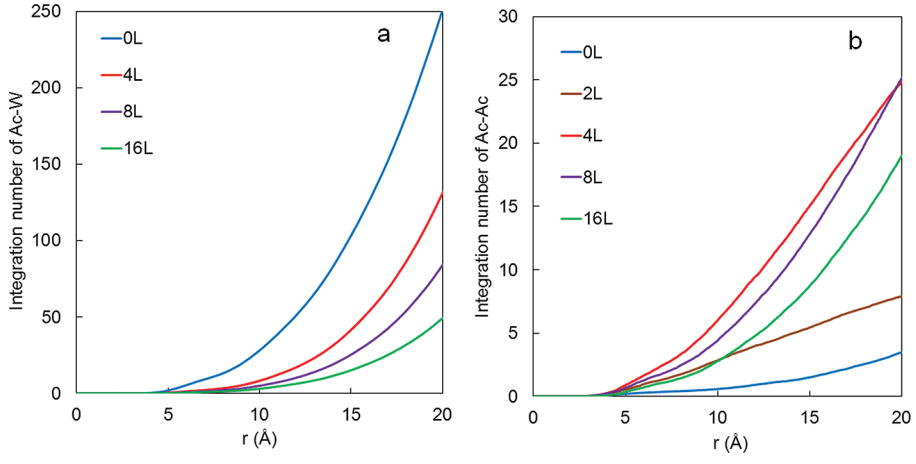

Figure 8. The running integration numbers for (a) Ac−W beads and (b) Ac−Ac beads of SPELA-*n*L macromonomers in 30% aqueous solution.

dx.doi.org/10.1021/jp211056p | J. Phys. Chem. B 2012, 116, 1536−1543

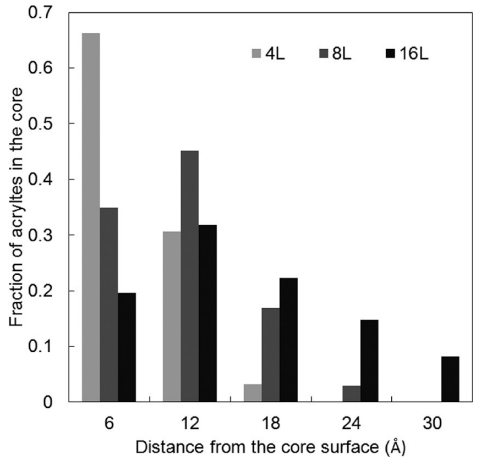

Figure 9. The distribution of Ac beads in the core of micelles for SPELA-*n*L macromonomers in 30% aqueous solution.

were positioned near the surface layer, away from the core's center. The average size of the micelles' core increased with *n*, which relaxed the volume constraint, thus increasing the fraction of acrylates in the core's inner layers. Therefore, the maximum fraction of Ac beads for macromonomers with $n = 8$ and $n = 16$ were located below the surface layer to minimize the interfacial free energy, as shown in Figure 9.

Figure 10 shows the variation of free and tethered fractions of acrylates with the number of lactides in each arm. All

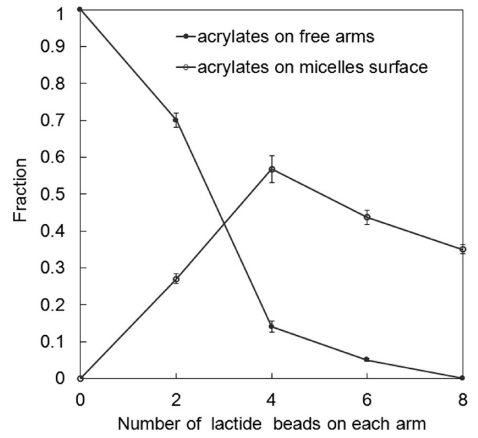

Figure 10. The effect of the number of lactide beads on each arm on the fraction of Ac beads on free arms and core surface of the micelles for SPELA-*n*L macromonomers in 30% aqueous solution. Error bars correspond to means ± 1 SD for $n = 5$ simulations.

acrylates were distributed uniformly in SPELA-0L. Increasing *n* led to the formation of larger micelles and a decrease in the fraction of free arms. The fraction of free arms decreased dramatically from 0.70 to 0.14 when *n* was increased from 2 to 4, which can be explained by a sharp increase in the volume to surface area ratio of the micelles. A 66% increase in the size of the lactide segment of the arms (*n* changing from 2 to 4) led to a 420% increase in the core volume of the micelles, while the number density of micelles decreased by only 10%. When *n* was increased to 8, almost all acrylates (>99%, see Figure 10) became part of the core volume of the micelles.

The reactive acrylate groups on SPELGA macromonomers cross-link by photopolymerization in aqueous solution and form mechanically robust hydrogel networks.[22] The covalent cross-links are stronger than the transient physical bridges between micelles. The reaction between the free acrylates, which are in contact with the aqueous phase, forms intermolecular cross-links and increases the cross-link density. The reaction between the acrylates in the micelle's core that belong to the same macromonomer (loops) increases the residence time of the bridges, while the reaction between those acrylates on different macromonomers (bridges) changes a transient bridge to a permanent cross-link. Since there is a high fraction of loops in the micelles' core (see the bridge fraction in Figure 7), a large fraction of the core acrylates undergo cyclization, which do not contribute to the elastic modulus of the network.

The effect of the number of lactide beads, *n*, on the reaction of acrylates and network formation can be divided into two regimes. SPELA-0L with 100% free acrylates produces networks with the highest and most uniform cross-link density. For low *n* values ($n \leq 4$), most of the acrylates are free (see Figure 7a) and the average distance between the acrylates in the micelles' core is relatively small (see Figure 3). Therefore, both free acrylates in the aqueous phase and core acrylates in the micelle phase contribute to network formation. With increasing *n*, the Ac−Ac integration number grows, which increases the rate of propagation reaction between the acrylates, leading to a reduction in gelation time (formation of infinite network). For $n > 4$, the fraction of free acrylates is negligible, so cross-linking is dominated by the reaction between the core acrylates. Since the solvent concentration in the micelle's core is very low, the core acrylates have significantly low diffusivity compared to free acrylates. Also, the average distance between the acrylates in the micelles' core increases with *n*. Thus, the rate of cross-linking decreases with increasing *n* for $n > 4$, leading to decreasing density of permanent bridges and lower elastic modulus of the network.

4. CONCLUSION

The mesoscale structure of the four-arm star poly(ethylene glycol-*co*-lactide)-acrylate (SPELA) macromonomer in aqueous solution was simulated by dissipative particle dynamics (DPD). The short lactide segments on each arm led to the formation of micelles. The micelle size, aggregation number (average number of macromonomers per micelle), and the number of intermicellar bridges increased with increasing number of lactides per arm. Among three possible conformations of the arms (free, loop, and bridge), the fraction of free arms decreased with increasing *n* while the fraction of loops decreased. The fraction of bridges showed a maximum at $n = 4$. There was a transition from the uniform distribution of acrylates for $n = 0$ to nearly complete incorporation in the micelles for $n > 4$. For the acrylates incorporated in the micelles, the fraction tethered to the core surface (those within a volume element facing the aqueous phase) decreased with increasing *n*. The average integration number of water beads around the acrylates was highest for the SPELA-0L ($n = 0$) and decreased with increasing *n*. The average integration number of acrylates around an acrylate had a biphasic behavior with a maximum at $n = 4$. The macromer concentration did not have a significant effect on the distribution of acrylates and the size of the micelles. The results predict that the conversion of SPELA-*n*L acrylates in the cross-linking reaction decreases with increasing *n*, thus reducing the modulus of the hydrogel. The results also predict that there is a trade-off between the hydrogel modulus and degradation with higher *n* values

dx.doi.org/10.1021/jp211056p | J. Phys. Chem. B 2012, 116, 1536−1543

favoring degradation. The predictions of the simulation can be used to design novel PEG-based hydrogels with robust mechanical properties and the desired degradation rate by changing the composition of the macromonomer.

AUTHOR INFORMATION

Corresponding Author

*Address: Department of Chemical Engineering, Swearingen Engineering Center, Rm 2C11, University of South Carolina, Columbia, SC 29208. Phone: (803) 777-8022. Fax: (803) 777-0973. E-mail: jabbari@cec.sc.edu.

Notes

The authors declare no competing financial interest.

ACKNOWLEDGMENTS

This work was supported by research grants to E.J. from the National Science Foundation under Grant Nos. CBET0756394, CBET0931998, and DMR1049381, the National Institutes of Health under Grant No. DE19180, and the Arbeitsgemeinschaft Fur Osteosynthesefragen (AO) Foundation under Grant No. C10-44J.

REFERENCES

(1) Cheng, Y. H.; Yang, S. H.; Su, W. Y.; Chen, Y. C.; Yang, K. C.; Cheng, W. T. K.; Wu, S. C.; Lin, F. H. *Tissue Eng., Part A* **2010**, *16*, 695.

(2) He, X. Z.; Jabbari, E. *Biomacromolecules* **2007**, *8*, 780.

(3) Peppas, N. A.; Lustig, S. R. *Solute diffusion in hydrophilic network structures, in hydrogels in medicine and pharmacy. I. Fundamentals*; CRC Press: 2004.

(4) Sarvestani, A. S.; He, X. Z.; Jabbari, E. *Biopolymers* **2007**, *85*, 370.

(5) Zhao, L. A.; Weir, M. D.; Xu, H. H. K. *Biomaterials* **2010**, *31*, 6502.

(6) Sarvestani, A. S.; He, X. Z.; Jabbari, E. *Biomacromolecules* **2007**, *8*, 406.

(7) Fu, Y.; Xu, K.; Zheng, X.; Giacomin, A. J.; Mix, A. W.; Kao, W. J. *Biomaterials* **2012**, *33*, 48.

(8) Adeloew, C.; Segura, T.; Hubbell, J. A.; Frey, P. *Biomaterials* **2008**, *29*, 314.

(9) Lee, P. J.; Langer, R.; Shastri, V. P. *J. Pharm. Sci.* **2005**, *94*, 912.

(10) Salinas, C. N.; Anseth, K. S. *J. Dent. Res.* **2009**, *88*, 681.

(11) Yan, C. Q.; Pochan, D. J. *Chem. Soc. Rev.* **2010**, *39*, 3528.

(12) Fu, S. Z.; Gun, G.; Gong, C. Y.; Zeng, S.; Liang, H.; Luo, F.; Zhang, X. N.; Zhao, X.; Wei, Y. Q.; Qian, Z. Y. *J. Phys. Chem. B* **2009**, *113*, 16518.

(13) Pollock, J. F.; Healy, K. E. *Acta Biomater.* **2010**, *6*, 1307.

(14) Bryant, S. J.; Anseth, K. S. *J. Biomed. Mater. Res., Part A* **2003**, *64A*, 70.

(15) Hawkins, A. M.; Milbrandt, T. A.; Puleo, D. A.; Hilt, J. Z. *Acta Biomater.* **2011**, *7*, 1956.

(16) Seck, T. M.; Melchels, F. P. W; Feijen, J.; Grijpma, D. W. *J. Controlled Release* **2010**, *148*, 34.

(17) Jeong, K. J.; Panitch, A. *Biomacromolecules* **2009**, *10*, 1090.

(18) Buwalda, S. J.; Dijkstra, P. J.; Calucci, L.; Forte, C.; Feijen, J. *Biomacromolecules* **2010**, *11*, 224.

(19) Jabbari, E.; He, X. *J. Mater. Sci. :Mater. Med.* **2008**, *19*, 311.

(20) Bae, Y. H.; Huh, K. M.; Kim, Y.; Park, K. H. *J. Controlled Release* **2000**, *64*, 3.

(21) Salaam, L. E.; Dean, D.; Bray, T. L. *Polymer* **2006**, *47*, 310.

(22) Moeinzadeh, S.; Khorasani, S. N.; Ma, J.; He, X.; Jabbari, E. *Polymer* **2011**.

(23) Clapper, J. D.; Skeie, J. M.; Mullins, R. F.; Guymon, C. A. *Polymer* **2007**, *48*, 6554.

(24) Leach, A. R. *Molecular modeling principles and applications*, 2nd ed.; Longman Press: London, 2001.

(25) Dotera, T.; Hatano, A. *J. Chem. Phys.* **1996**, *105*, 8413.

(26) Groot, R. D.; Madden, T. J. *J. Chem. Phys.* **1998**, *108*, 8713.

(27) van Vlimmeren, B. A. C.; Maurits, N. M.; Zvelindovsky, A. V.; Sevink, G. J. A.; Fraaije, J. G. E. M. *Macromolecules* **1999**, *32*, 646.

(28) Hoogerbrugge, P. J.; Koelman, J. M. V. A. *Europhys. Lett.* **1992**, *19*, 155.

(29) Espanol, P.; Warren, P. *Europhys. Lett.* **1995**, *30*, 191.

(30) Guo, X. D.; Zhang, L. J.; Qian, Y.; Zhou, J. *Chem. Eng. J.* **2007**, *131*, 195.

(31) Guo, X. D.; Zhang, L. J.; Wu, Z. M.; Qian, Y. *Macromolecules* **2010**, *43*, 7839.

(32) Scocchi, G.; Posocco, P.; Fermeglia, M.; Pricl, S. *J. Phys. Chem. B* **2007**, *111*, 2143.

(33) Thakkar, F. M.; Ayappa, K. G. *J. Phys. Chem. B* **2010**, *114*, 2738.

(34) Groot, R. D.; Madden, T. J.; Tildesley, D. J. *J. Chem. Phys.* **1999**, *110*, 9739.

(35) Flory, P. J. *Principles of Polymer Chemistry*; Cornell University Press: New York, 1953.

(36) Groot, R. D.; Warren, P. B. *J. Chem. Phys.* **1997**, *107*, 4423.

(37) Cao, X. R.; Xu, G. Y.; Li, Y. M.; Zhang, Z. Q. *J. Phys. Chem. A* **2005**, *109*, 10418.

(38) Posocco, P.; Fermeglia, M.; Pricl, S. *J. Mater. Chem.* **2010**, *20*, 7742.

(39) Wang, Y. C.; Lee, W. J.; Ju, S. P. *J. Chem. Phys.* **2009**, *131*.

(40) Zhao, Y.; You, L. Y.; Lu, Z. Y.; Sun, C. C. *Polymer* **2009**, *50*, 5333.

(41) Xia, J.; Zhong, C. L. *Macromol. Rapid Commun.* **2006**, *27*, 1110.

(42) Xu, Y.; Feng, J.; Liu, H.; Hu, Y. *Mol. Simul.* **2006**, *32*, 375.

(43) Groot, R. D.; Rabone, K. L. *Biophys. J.* **2001**, *81*, 725.

(44) Loverde, S. M.; Ortiz, V.; Kamien, R. D.; Klein, M. L.; Discher, D. E. *Soft Matter* **2010**, *6*, 1419.

(45) Ortiz, V.; Nielsen, S. O.; Discher, D. E.; Klein, M. L.; Lipowsky, R.; Shillcock, J. *J. Phys. Chem. B* **2005**, *109*, 17708.

(46) Sun, H. *J. Phys. Chem. B* **1998**, *102*, 7338.

(47) Flory, P. J. *Statistical mechanics of chain molecules*; Interscience: New York, 1969.

(48) Choi, Y. R.; Bae, Y. H.; Kim, S. W. *Macromolecules* **1998**, *31*, 8766.

(49) Devanand, K.; Selser, J. C. *Macromolecules* **1991**, *24*, 5943.

(50) *Materials Studio V 5.5*; Accelrys Inc.: San Diego, CA, 2011.

(51) Nagarajan, R. *Langmuir* **2002**, *18*, 31.

(52) Tanford, C. *The hydrophobic effect: formation of micelles and biological membranes*, 2nd ed.; John Wiley & Sons: New York, 1980.

(53) Nicolai, T.; Colombani, O.; Chassenieux, C. *Soft Matter* **2010**, *6*, 3111.

(54) Sliozberg, Y. R.; Andzelm, J. W.; Brennan, J. K.; Vanlandingham, M. R.; Pryamitsyn, V.; Ganesan, V. *J. Polym. Sci., Part B: Polym. Phys.* **2010**, *48*, 15.

(55) Fioroni, M.; Burger, K.; Mark, A. E.; Roccatano, D. *J. Phys. Chem. B* **2001**, *105*, 10967.

(56) Hansen, J. P.; McDonald, I. R. *Theory of simple liquids*, 2nd ed.; Academic Press: London, 1990.